CHAPTER 3
MODELLING AND ANALYSIS OF COMBINED REHEAT RENEGERATIVE VAPOUR POWER CYCLE (RRVPC) AND SINGLE EFFECT H_2O–LiBr VARS

3.1 Introduction

As discussed in Chapter 2, there are lots of studies available in the literature on VARS performance analysis. Most of these research works specific to (i) thermo–physical properties of various working fluid pairs, (ii) first law based VARS performance analysis (iii) exergy analysis of single and multi-effect VARS, (iv) thermo–economic analysis and optimization were discussed topic wise in Chapter 2. Since a VARS is operated with low grade heat energy, therefore, in some studies, VARS performance analysis is provided along with the analysis of the heat providing topping solar/GT/MGT/ICE cycle. Studies related to thermodynamic performance analysis of solar/GT/MGT/ICE driven CPC systems were also a major part of the literature review section in Chapter 2 including review on binary mixture based CPC system with different heat sources. Thermodynamic studies performed on some VPC based steam power plants were also reviewed and discussed separately in Chapter 2. From the comprehensive review in Chapter 2, it was found that there is no research study available on a combined cogeneration system that involves a combination of the ST based VPC as topping cycle and the H_2O–LiBr VARS as bottoming cycle.

In thermal power plants, where steam is produced in abundance, sometimes is lost unused at some intermediate/low pressure. Steam is a good heating medium and most commonly used as a heat source for the VARS [1–3]. In this chapter, a novel combined reheat regenerative type VPC (RRVPC) and a single effect H_2O–LiBr VARS is considered for thermodynamic analysis. Detail thermodynamic modelling of the proposed CPC system is elaborately presented. Steam extracted from the ST of the topping reheat regenerative vapour power cycle (RRVPC) is the source of heat for the VARS generator. Energy based parametric analysis of the proposed CPC system is performed based on variation of some operating parameters of the topping RRVPC and bottoming single effect H_2O–LiBr VARS. Additionally, a comparative performance analysis is also carried out to quantify the difference in system performance with and without VARS in the bottoming cycle.

3.2 Description of the combined RRVPC and single effect H_2O–LiBr VARS

The schematic of the combined RRVPC and the single effect H_2O–LiBr VARS is shown in Fig. 3.1. The VPC employs one open feed water heater (OWH); one closed feed water heater (CWH) and a reheater. The bottoming cycle is a single effect H_2O–LiBr VARS. The single effect VARS consists of the generator, condenser, expansion valve, evaporator, absorber, solution pump (SP), SHE and a throttle valve. The topping VPC uses a coal fired boiler for steam generation. The high pressure superheated steam produced in the boiler enters the steam turbine (ST) which is first expanded to a pressure of 0.2 times of the boiler pressure. At this pressure, some steam is extracted for the CWH and remaining steam is reheated at the same pressure to the original superheated temperature. Some amount of steam is also extracted from the ST at an intermediate pressure for the OWH. Steam for the VARS generator is extracted at a lower pressure which solely depends on the specified generator temperature. Remaining steam expands to the condenser pressure and is completely condensed in the condenser. The steam that condenses in the VARS generator is pumped to increase its pressure to OWH pressure where it mixes the feed water at the same pressure and heated to the saturation temperature corresponding to the pressure of the OWH. The mixture is then pumped to the boiler pressure which again mixes with the high pressure condensed water from the CWH at the same boiler pressure. Cold water from the cooling tower (CT) basin is supplied to the condenser of the VPC and also to the condenser, absorber and evaporator of the single effect VARS. The chilled water from the VARS evaporator passes through the air conditioning (AC) apparatus before it mixes with return hot water streams from condenser of the VPC, condenser and absorber of the VARS in the mixing chamber. The mixed hot water stream is pumped to the wet CT for cooling of water by air. The cold water from the CT is then again routed through condenser of the steam cycle, condenser, absorber, evaporator and AC apparatus of the VARS using another pump at the exit of the CT basin.

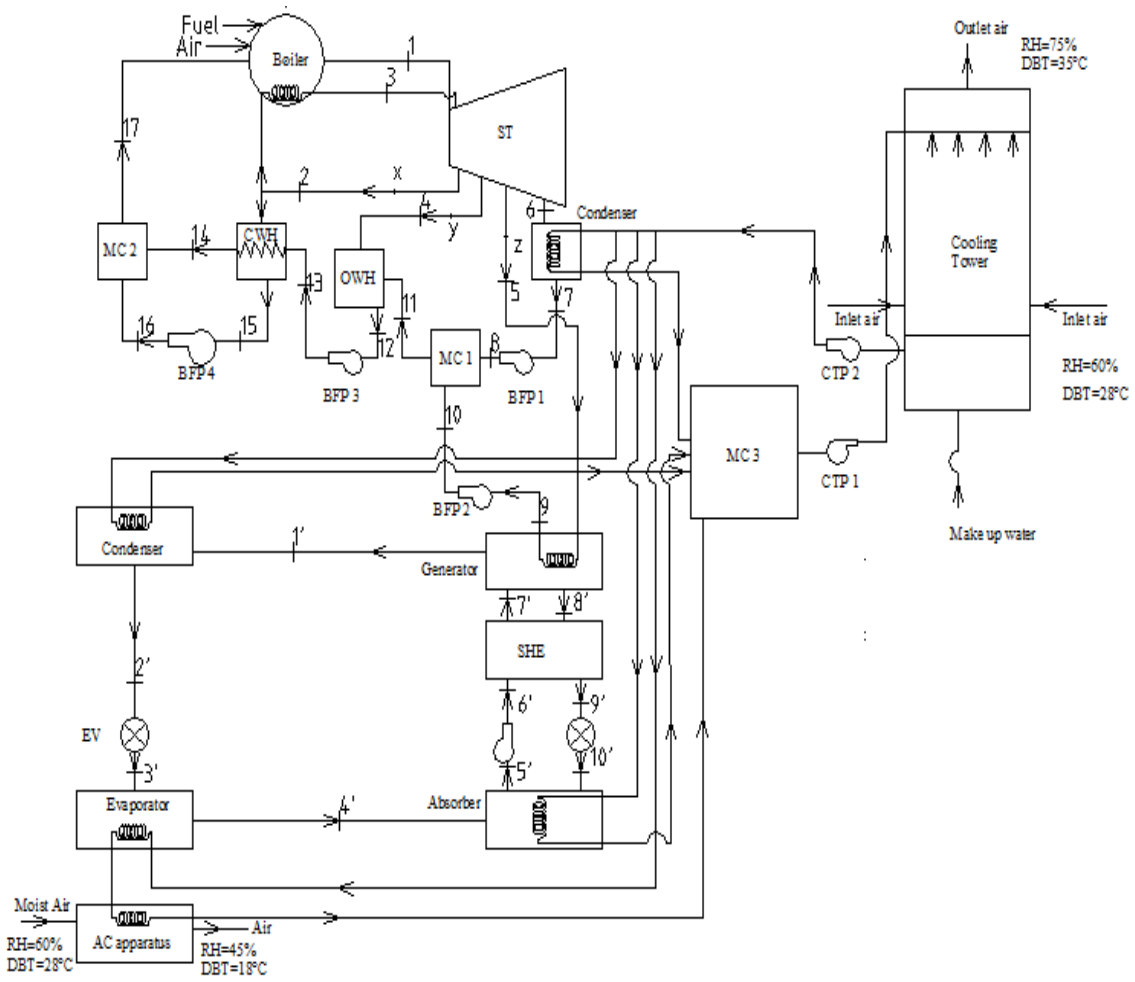

Fig. 3.1: Schematic of the combined RRVPC and single effect H_2O–LiBr VARS

3.3 Assumptions and few preliminary calculations

The coal used in the boiler has the following chemical composition (ultimate analysis). Carbon (C) 60%, Hydrogen (H_2) 4%, Oxygen (O_2) 3%, Nitrogen (N_2) 2%, Sulphur (S) 3%, Moisture (H_2O) 4% and Ash content 24%. Complete combustion of coal is assumed with flue gas comprising of only carbon–di–oxide (CO_2), sulfur–di–oxide (SO_2), water vapor (H_2O) and nitrogen. It is assumed that fuel and air bound oxygen is just sufficient to completely oxidize the combustible elements in the fuel and hence no oxygen in the product flue gas. Ash in the flue gas is also neglected. The following complete combustion equations are used.

$$n_C\left(C + O_2 \rightarrow CO_2\right) \tag{3.1}$$

$$n_{H_2}\left(H_2+\frac{1}{2}O_2\rightarrow H_2O\right) \tag{3.2}$$

$$n_s\left(S+O_2\rightarrow SO_2\right) \tag{3.3}$$

where, $n_C=\frac{C}{M_C}$, $n_{H_2}=\frac{H_2}{M_H}$, $n_S=\frac{S}{M_S}$, are the molar composition of C, H_2 and S per 100 kg of fuel. M_C, M_{H_2} and M_S are the respective molecular weights. Determination of flue gas composition is straightforward from the above equations [4]. However, for H_2O and N_2 in the flue gas, the fuel bound molar amounts are also taken into consideration.

The no of moles of air bound O_2 required per 100 kg of fuel is:

$$n_{O_2}=n_C+\frac{1}{2}n_{H_2}+n_S-n_{O_{2,f}} \tag{3.4}$$

where, $n_{O_{2,f}}$ is the no of moles of fuel bound oxygen per 100 kg of fuel. Thus knowing the fuel mass flow rate, the flow rate of air required for complete combustion of coal can be determined.

It is assumed that the steam generated in the boiler is superheated at 500°C irrespective of the boiler pressure which in the present analysis is varied from 100 to 200 bars to evaluate its effect on net power and efficiency of the reheat regenerative Rankine cycle. The reheat/CWH pressure is assumed 0.2 times the boiler pressure, hence the corresponding saturation temperature is known. The pressure in the OWH is however determined from the condition of maximum efficiency as given by the following equation [5].

$$T_x=\frac{(T_b-T_c)}{N+1} \tag{3.5}$$

where, T_x =temperature rise per heater for maximum efficiency

T_b =saturation temperature corresponding to boiler pressure (Pb)

T_c =saturation temperature corresponding to condenser pressure (Pc)

N = number of feed water heaters which in the present cycle is 2 (one OWH and one CWH)

T_x is the difference between the temperature at point 2s and 4s in the T–s diagram (Fig. 3.2).

$$T_x = T_{2s} - T_{4s} \tag{3.6}$$

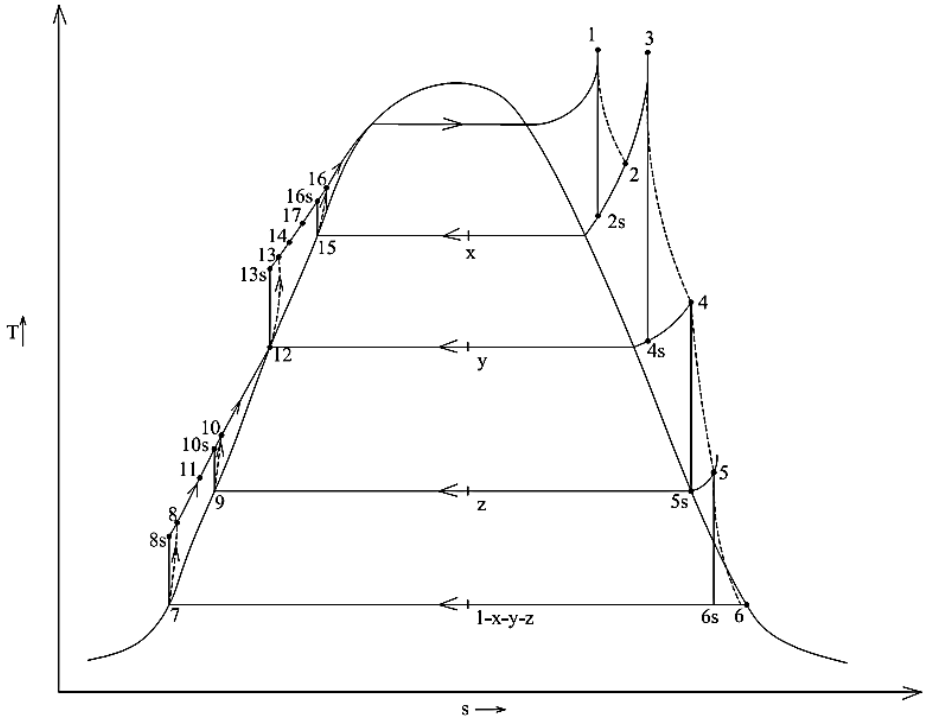

Fig. 3.2: Rankine cycle T–s diagram

Eq. (3.6) gives the value of T_{4s} and the corresponding pressure in the OWH. The pressure corresponding to state 5s (also state 5) is selected based on generator temperature of the VARS. A temperature difference of 10 $^{\circ}$C is considered between the generator temperature and saturation temperature of steam extracted to the generator and accordingly the pressure at state 5 gets fixed. A terminal temperature difference (TTD) of 3 $^{\circ}$C is assumed in the CWH i.e.

$$T_{14} = T_{15} - TTD \tag{3.7}$$

Steady flow assumptions have been made neglecting the kinetic and potential energy effects. Some of the assumed parameters, efficiency and effectiveness of the components of the combined system are shown in Table 3.1.

Table 3.1: Assumed values of parameters

Parameter	Value
ST isentropic efficiency	85%
Pump isentropic efficiency	85%
Boiler pressure	Variable(100 to 200 bar)
Reheat pressure	0.2 times of boiler pressure
Condenser pressure	0.1 bar
Terminal temperature difference in CWH	3 $^{\circ}$C
Cooling tower exit water temperature	25 $^{\circ}$C
Flue gas temperature at boiler exit	300 $^{\circ}$C
VARS condenser exit water temperature	30 $^{\circ}$C
VARS absorber exit water temperature	30 $^{\circ}$C
VARS evaporator exit water temperature	10 $^{\circ}$C
Chilled water temperature at AC apparatus inlet	10 $^{\circ}$C
CT inlet air temperature	28 $^{\circ}$C
CT inlet air relative humidity	60%
CT exit air temperature	35 $^{\circ}$C
CT exit air relative humidity	75%
Air mass flow rate through AC apparatus	4 kg/s
AC apparatus inlet air temperature	28 $^{\circ}$C
AC apparatus exit air temperature	18 $^{\circ}$C
AC apparatus inlet air relative humidity	60%
AC apparatus exit air relative humidity	45%
SHE effectiveness	75%

3.4 Thermodynamic modelling of the RRVPC and VARS based CPC system

3.4.1 Thermodynamic modelling of the topping RRVPC

The specific enthalpy and entropy at all the salient points of the Rankine cycle has been calculated. Steady flow energy equation (SFEE) is applied to the various system components for the purpose of finding work and heat transfer terms wherever applicable.

Application of SFEE to various components gives:

For the CWH, $x(h_2 - h_{15}) = (1-x)(h_{14} - h_{13})$ (3.8)

For the OWH, $yh_4 + (1-x-y)h_{11} = (1-x)h_{12}$ (3.9)

For mixing chamber 1, $(1-x-y)h_{11} = zh_{10} + (1-x-y-z)h_8$ (3.10)

For mixing chamber 2, $h_{17} = (1-x)h_{14} + xh_{16}$ (3.11)

Work produced by ST per kg of steam,

$$W_{ST} = (h_1 - h_2) + (1-x)(h_3 - h_4) + (1-x-y)(h_4 - h_5) + (1-x-y-z)(h_5 - h_6) \quad (3.12)$$

Total pump work required for running the boiler feed pumps of the VPC per kg of steam is:

$$W_{BFP} = (1-x-y-z)(h_8 - h_7) + z(h_{10} - h_9) + (1-x)(h_{13} - h_{12}) + x(h_{16} - h_{15}) \quad (3.13)$$

x, y and z in the above equations are fraction of steam extracted per kg of steam for the CWH,OWH and generator of the VARS.

The mass flow rate of steam produced in the boiler is calculated from the energy balance applied to the boiler control volume.

$$\dot{m}_s = \frac{\dot{m}_f LHV_f - \dot{E}_{fg}}{(h_1 - h_{17}) + (1-x)(h_3 - h_2)} \quad (3.14)$$

$\dot{m}_f$ is the fuel mass flow rate (a model input parameter) and LHV_f is the lower heating value of coal calculated as follows [4]. $\dot{E}_{fg}$ is the energy lost with the flue gas at the exhaust temperature.

$$LHV_f = -\left[\frac{\sum_P n\bar{h}_d^0 - \sum_R n\bar{h}_d^0}{100}\right] \tag{3.15}$$

In the above equation, *n* corresponds to the molar coefficients of products (*P*) and reactants (*R*) per 100 kg of fuel. $\bar{h}_d^0$ is the standard molar specific enthalpy of devaluation, its value for various substances are known and available in Refs. [4, 6]. The energy lost with the flue gas is calculated using the following equation.

$$\dot{E}_{fg} = \frac{\dot{m}_f}{100}\sum_{i=1}^{n} n_i \Delta\bar{h}_i \tag{3.16}$$

In the above equation, $\Delta\bar{h}_i$ is enthalpy change of the i^{th} flue gas product corresponding to the states of flue gas exhaust temperature (T_g) and the reference temperature (T_0). This is expressed as $\Delta\bar{h} = \bar{h}(T_g) - \bar{h}(T_0)$. n_i is the molar amount of the i^{th} component in the flue gas per 100 kg of fuel. n is the number of products considered in the flue gases.

The calculations for the CT, CT side pumps and the AC apparatus depends upon the working of the bottoming VARS, hence these are shown in the section below.

3.4.2 Thermodynamic modelling of the bottoming single effect H_2O–LiBr VARS

In the VARS, we consider a single effect H_2O–LiBr absorption system consisting of a SHE. Concentration of the strong and weak solution of the refrigerant as functions of operating temperatures is known [7].

$$X_{ss} = \frac{49.04 + 1.125T_A - T_E}{134.65 + 0.47T_A} \tag{3.17}$$

$$X_{ws} = \frac{49.04 + 1.125T_G - T_C}{134.65 + 0.47T_G} \tag{3.18}$$

Thermodynamic properties such as specific enthalpy, entropy of the refrigerant (water) both in liquid and vapour state at various pressures and temperature are determined from International Associations for the properties of water and steam (IAPWS) formulation 1997 [8]. Similarly the thermodynamic properties of H_2O–LiBr solutions at various temperatures and concentration are calculated using the correlations proposed by Patek and Klomfar [9].

The cooling load (CL) in the evaporator ($\dot{Q}_E$) is an input to the thermodynamic model from which the mass flow rate of refrigerant can be determined as given below.

$$\dot{m}_{H_2O} = \frac{\dot{Q}_E}{h_4' - h_3'} \tag{3.19}$$

The mass flow rate of strong and weak solution is calculated from the following equations [7].

$$\dot{m}_{ss} = \frac{\dot{m}_{H_2O} X_{ws}}{X_{ws} - X_{ss}} \tag{3.20}$$

$$\dot{m}_{ws} = \frac{\dot{m}_{H_2O} X_{ss}}{X_{ws} - X_{ss}} \tag{3.21}$$

The thermal load in the generator, absorber and condenser can be expressed as:

$$\dot{Q}_G = \dot{m}_{H_2O} h_1' + \dot{m}_{ws} h_8' - \dot{m}_{ss} h_7' \tag{3.22}$$

$$\dot{Q}_A = \dot{m}_{H_2O} h_4' + \dot{m}_{ws} h_{10}' - \dot{m}_{ss} h_5' \tag{3.23}$$

$$\dot{Q}_C = \dot{m}_{H_2O} \left(h_1' - h_2' \right) \tag{3.24}$$

The heat required for vapour generation in the generator is supplied by steam extracted from the topping vapour power cycle. Mass of steam extracted for the purpose is found out from the following equation.

$$\dot{m}_{s,extracted} = \frac{\dot{Q}_G}{h_5 - h_9} \tag{3.25}$$

Similarly, $\dot{Q}_E$, $\dot{Q}_C$ and $\dot{Q}_A$ values give the mass flow rate of cooling water to be passed through these devices from heat balance applied to these devices.

For the AC apparatus, it is considered that the atmospheric air enters the AC at 28°C and 60% relative humidity and moist air exits the apparatus at 18°C and 45% relative humidity. Specific humidity and specific enthalpy of moist air (per kg of dry air) of moist air are calculated using the following equations.

$$\omega = 0.622 \frac{p_w}{p_{atm} - p_w} \tag{3.26}$$

$$h = 1.005 t_{db} + \omega(2500 + 1.88 t_{db}) \tag{3.27}$$

In the above equations, p_w, t_{db} and ω are the partial pressure of water vapour, dry bulb temperature and specific humidity of moist air. Neglecting losses, energy balance in the AC apparatus gives:

$$\dot{m}_{w,AC} C_{pw} (T_{w,o} - T_{w,i}) = \dot{m}_{a,AC} \left[(h_{a,i} - h_{a,o}) - (\omega_i - \omega_o) h_{f,o} \right] \tag{3.28}$$

where, $\dot{m}_{w,AC}$ and $T_{w,i}$ are the mass flow rate of chilled water and its temperature at entry to the AC apparatus, which are known and equal to values at the evaporator exit state. The water temperature at AC apparatus exit '$T_{w,o}$' is calculated from the above equation. The water from the VPC condenser and condenser, absorber of the single effect VARS and the AC apparatus, all goes to a mixing chamber 3 (MC3). The temperature of the mixed water stream is calculated from the SFEE applied to the mixing chamber.

3.4.3 CT side pumping power and system efficiency calculation

The same principle of heat and mass transfer (as applied in the AC apparatus) is applied in the CT for calculating air flow rate required to achieve the cooling of water to the desired temperature. Unlike for the boiler feed pumps (BFPs); the pumping power calculation for the CT side pumps is done in a different way. The parameters such as pipe diameter, length, static lift etc. used for the calculation are given in Table 3.2. The *k* value for the elbow and valve are taken 0.75 and 0.19 respectively. Friction factor is approximated using the Swamee–Jain equation.

$$f = 0.25 \frac{1}{\log\left(\left(\frac{\varepsilon}{3.7D}\right) + 5.74\,\mathrm{Re}^{-0.9}\right)^2} \tag{3.29}$$

This equation is valid for $10^{-6} < \frac{\varepsilon}{D} < 10^{-2}$ and $3000 < R_e < 3\times10^{8}$. Kinematic viscosity and density values of water are taken at 25°C with $\nu_{water} = 0.892\times10^{-6}$ m^2/s; $\rho_{water} = 997.075\,\mathrm{Kg/m^3}$. Commercial steel pipes with roughness height, $\varepsilon = 4.5\times10^{-5}$ m is used.

The efficiency of reheat regenerative Rankine cycle and also the overall efficiency of the combined power and cooling system (considering losses with flue gas exhaust in the boiler) are determined using the following equations.

$$\eta_{Rankine} = \frac{\dot{m}_s\left(W_{ST} - W_{BFP}\right) - \dot{m}_{w,CTP}W_{CTP}}{\dot{m}_s\left[\left(h_1 - h_{17}\right) + \left(1-x\right)\left(h_3 - h_2\right)\right]} \tag{3.30}$$

$$\eta_{Overall} = \frac{\dot{m}_s\left(W_{ST} - W_{BFP}\right) - \dot{m}_{w,CTP}W_{CTP}}{\dot{m}_f LHV_f} \tag{3.31}$$

Table 3.2: Assumed values of parameters used for CT side pumping power calculation

	Pipe diameter (m)	Length (m)	Static lift (m)	Frictional loss in components (m)	No. of valves	No. of Elbows
1. For the pipe segments through Rankine cycle steam condenser connecting the cooling tower basin and the mixing chamber	0.6096	28.5 2 2 2 15	2	9	4	3
2. For the pipe through evaporator and A/C apparatus leading to the mixing chamber	Calculated	120	2	10	3	6
3. For the pipe through absorber leading to the mixing chamber	Calculated	80	2	5	3	4
4. For the pipe through VARS condenser leading to the mixing chamber	Calculated	80	2	5	3	4
5. For the pipe connecting the mixing chamber and the cooling tower	0.6096	25	3		1	2

3.5 Validation of VPC and single effect VARS models

To validate the computer code developed for simulating the toping VPC and bottoming single effect VARS, the results obtained from the computer code were compared with those of Ref. [11] which was done for a reheat steam power cycle with open water heater. In the present study, the properties of water and steam were calculated using equations taken from Ref. [8]. From the comparison shown in Table 3.3, it is seen that the computer code generates almost the same results with those of Ref. [11] for the reheat steam power cycle with one open water heater. This ensures the correct use of the model equations taken from Ref. [11]. Similarly to validate the model developed for simulating the bottoming single effect VARS, the results obtained from the computer code was compared with those of Lansing [7] under same operating conditions. The comparison is shown in Table 3.4 and the results show a satisfactory agreement. Slight deviations in the results is due to the fact that some of the modeling equations used in the present study were taken from Patek and Klomfar [9] which are different from those of Lansing [7]. Since the results obtained from the VPC and VARS model don't deviate much from those of Ref. [11] and Ref. [7], therefore, the models were further modified to simulate the proposed combined RRVPC and single effect VARS. The results obtained from simulation of the proposed combined RRVPC and VARS based are presented in the following subsections.

Table 3.3: Validation of results obtained from the computer code written for simulating a reheat steam power cycle with those of Ref. [11] at same operating conditions (Pump and turbine isentropic efficiency=90%)

State	Ref. [11]				Results obtained from computer code			
	T(°C)	P(bar)	*h* (kJ/kg)	*s* (kJ/kgK)	T(°C)	P(bar)	*h* (kJ/kg)	*s* (kJ/kgK)
1	500	120	3348	6.487	500	120	3350	6.4902
2	–	24	2957	6.569	277.54	24	2957.5	6.5707
3	500	24	3463	7.343	500	24	3463.7	7.345
4	–	1.5	2813	7.513	170.25	1.5	2813.7	7.515
5	39	0.07	2399	7.720	39.0	0.07	2382.5	7.668
6	39	0.07	163.4	0.5591	39.0	0.07	163.365	0.5591
7	–	1.5	163.5	0.5592	39.025	1.5	163.526	0.5593
8	–	1.5	462.8	1.4225	111.35	1.5	467.081	1.4335
9	–	120	474.3	1.4254	112.593	120	480.942	1.4372
Steam extracted (kg/s)			0.113				0.1145	
Net power (kJ/kg of			1408				1410.3	
Heat supplied (kJ/kg of			3380				3375.2	
Efficiency (%)			41.66				41.78	

Table 3.4: Validation of results obtained from simulation of the single effect water-LiBr VARS with those of Ref. [7] at same operating conditions (Evaporator heat load $\dot{Q}_E$ =3.5112 kW, $T_G = 90\,°C$, $T_E = 7\,°C$, $T_A = 40\,°C$ and $T_C = 40\,°C$, SHE efficiency = 80%)

Parameter	Ref. [7]	Present study
Generator heat load, ($\dot{Q}_G$ kW)	4.5247	4.5999
Condenser heat load, ($\dot{Q}_C$ kW)	3.7414	3.7432
Absorber, ($\dot{Q}_A$ kW)	4.2945	4.368
Evaporator pressure (kPa)	0.9933	1.0021
Condenser pressure (kPa)	7.3821	7.3844
Weak solution concentration (X_{ws})	0.6233	0.6233
Strong solution concentration (X_{ss})	0.5672	0.5672
Refrigerant mass flow rate (kg/s)	0.0015	0.0015
Weak solution mass flow rate (kg/s)	0.0151	0.0151
Strong solution mass flow rate (kg/s)	0.0166	0.0166
COP	0.776	0.7633

3.6 Thermodynamic analysis of the combined VPC and VARS

The simulation results of the proposed combined RRVPC and the H_2O–LiBr VARS are presented in this section. The fuel (coal) flow rate is varied from 5 kg s^{-1} to 20 kg s^{-1} and the boiler pressure from 100 to 200 bar to investigate the effect of these two parameters on performance of the toping reheat regenerative ST cycle. During boiler pressure variation, the fuel flow rate is kept fixed at 20 kg s^{-1} while during fuel flow rate variation; the boiler pressure is kept constant at 150 bar. The temperature in the generator, condenser, evaporator and absorber of the bottoming VARS are maintained at 80°C, 35°C, 10°C and 35°C respectively during these variations with evaporator CL maintained at 4000 tons of refrigeration (TOR). For the VARS, parametric study has been carried to investigate the effect of operating parameters such as generator temperature, condenser temperature, evaporator temperature, absorber temperature and evaporator CL on coefficient of performance and thermal loads of various components. During variation of these parameters the boiler pressure is maintained at 150 bar while the fuel flow rate at 20 kg s^{-1}. Mass flow rate of refrigerant (water), LiBr salt, weak and strong solution of the refrigerant are determined at various operating conditions. Further a comparison of net power, efficiency of the combined cycle is made with only the topping ST cycle without VARS. Comparison of efficiency, power and steam generation rate (SGR) of the ST cycle without VARS is also provided against the ST cycle without CWH.

3.6.1 Effect of boiler pressure on ST cycle power, efficiency and steam generation rate

The effect of boiler pressure on power, steam generation rate and efficiency of the topping cycle is shown in Figs. 3.3(a) and 3.3(b).

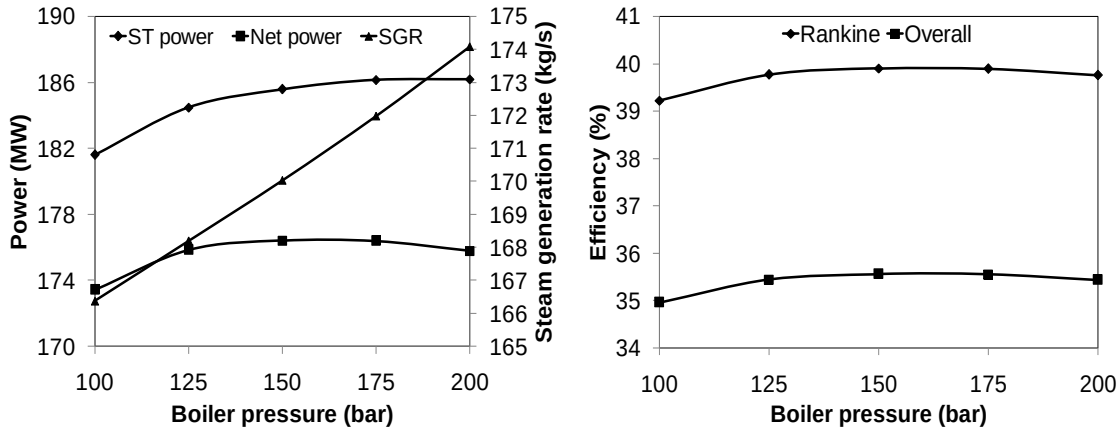

(a) (b)

Fig. 3.3: Effect of boiler pressure on (a) power and SGR (b) efficiency of the topping ST cycle

As seen in Fig. 3.3(a), the ST power increases rapidly at the beginning with increase in boiler pressure which however becomes gradual towards the end. During boiler pressure variation from 100 to 200 bar, due to temperature of superheated steam at ST inlet which is fixed at 500°C, it results in change of state of working fluid (steam/water) at inlet and exit of the high pressure (HP) and low pressure (LP) stages of the ST and also in the other state points of the cycle. It certainly affects the power output from the ST, but what is more significant is the increase in the steam generation rate with boiler pressure. The combined effect of these two factors is ultimately responsible for the ST power obtained at various boiler pressures. More steam is generated at higher boiler pressure; increase in steam generation rate is directly proportional to the boiler pressure as shown in Fig. 3.3(a). Difference in enthalpy of steam between state points 1 and 17 and also between 2 and 3 reduces and hence steam generation capacity of boiler increases at higher boiler pressure (due to fixed inlet temperature condition at HP ST). On the other hand, the net power although initially increases with boiler pressure but later on at higher boiler pressure, the increase becomes gradual and shows a decreasing

trend at boiler pressure above 175 bar. This is due to the total pumping power requirement for the BFPs and CT side pumps which also increases with boiler pressure. And the increase in pumping power requirement is more compared to the corresponding gain in the ST power at higher boiler pressure. From Fig. 3.3(b), we see that the efficiency of the reheat regenerative Rankine cycle and the overall efficiency both vary very little with boiler pressure. Maximum net power and overall system efficiency is obtained at boiler pressure of 150 bar.

3.6.2 Effect of fuel mass flow rate on ST cycle power, efficiency and steam generation rate

Figs. 3.4(a) and 3.4(b) show the effect of fuel mass flow rate on SGR, power and efficiency. When the rate of fuel supply to the boiler furnace is increased, the steam generation capacity of the boiler increases (Fig 3.4(a)). This is obvious because more fuel burns releasing higher amount of energy and also since the boiler pressure and the flue gas exhaust temperature are fixed, so a direct increase in the numerator of Equation (14) causes increase in SGR$(\dot{m}_s)$. Accordingly, the ST power and the net power also show an increasing trend with fuel flow rate (Fig. 3.4(a)). Total pumping power requirement also increases with increase in fuel flow rate. This can be observed from a wider gap between the ST power and net power line at higher fuel flow rate. The increase is more in case of CT side pumping power requirement than in case of BFPs. The efficiencies of the combined power and cooling plant is however not affected much by increase in the fuel flow rate as it is shown in Fig. 3.4(b). Although due to increase in fuel flow rate, the steam generation capacity and net plant power increase but fuel energy supplied in the boiler also increases simultaneously, therefore it affects the system efficiency accordingly.

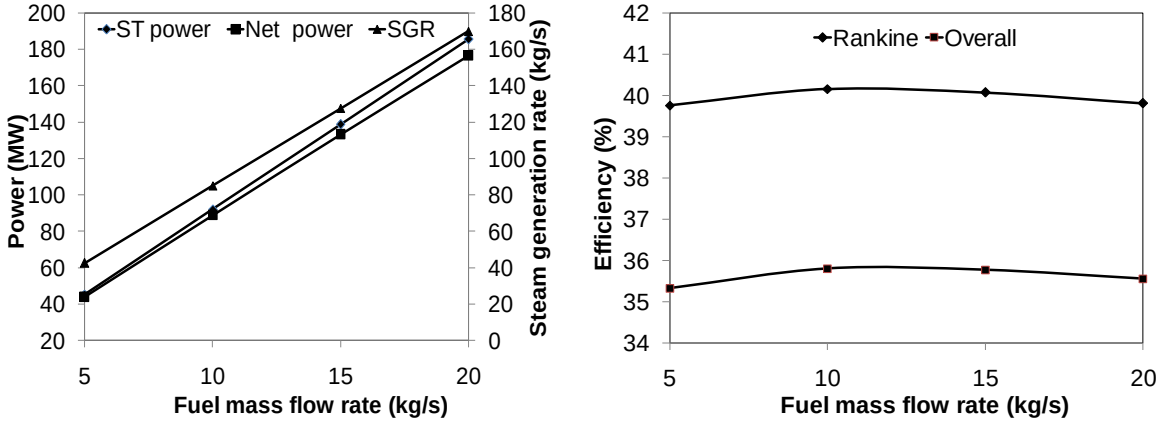

(a) (b)

Fig. 3.4: Effect of fuel mass flow rate on (a) power, SGR and (b) efficiency of the topping ST cycle

3.6.3 Effect of evaporator CL on performance of ST cycle and VARS

When the VARS evaporator CL is increased keeping the other parameters fixed, the ST power reduces slightly, but compared to this, the reduction in net power of the combined plant is more (Fig. 3.5(a)). This is due to the mass flow rate of steam extracted from the ST which increases with the evaporator CL as shown in Fig. 3.5(a). The pumping power requirement for the BFPs is not affected (slightly reduces with TOR), however the CT side pumping power increases significantly due to increase in the water mass flow rate resulting from increase in evaporator CL. Hence the net power shows a decreasing trend. As a result, the Rankine cycle and the overall cycle efficiency also reduces marginally, however the impact is less on efficiency as depicted in Fig. 3.5(b).

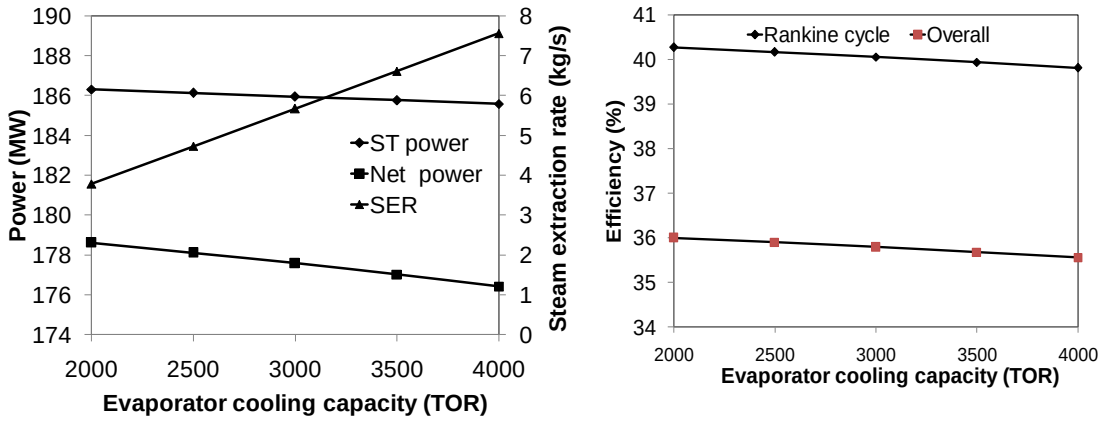

(a) (b)

Fig. 3.5: Effect of VARS evaporator CL on (a) power, steam extraction rate (SER) and (b) efficiency of the topping ST cycle

With increase in evaporator CL, the thermal load in all the components of the VARS increases proportionately (Refer Table 3.5). The SP power also increases linearly with CL. However, the enthalpy at various state points is not affected by the change in CL. Although the thermal load in the generator ($\dot{Q}_G$), evaporator ($\dot{Q}_E$) and the SP power increases with CL, but the COP value remains unchanged and this may be due to proportional increase of the above parameters. The COP value at all TORs is 0.813.

From Table 3.5 it is also observed that the mass flow rate of refrigerant (water), lithium bromide salt, weak and strong solution; all increases with evaporator CL.

Table 3.5: Variation of performance parameters of the H_2O–LiBr VARS with evaporator cooling load

TOR	$\dot{Q}_G$ (MW)	$\dot{Q}_A$ (MW)	$\dot{Q}_C$ (MW)	$\dot{Q}_E$ (MW)	$\dot{m}_{H_2O}$ (kg/s)	$\dot{m}_{LiBr}$ (kg/s)	$\dot{m}_{ws}$ (kg/s)	$\dot{m}_{ss}$ (kg/s)	SP power (Watt)
2000	8.614	8.228	7.386	7	2.95	10.874	18.004	20.954	59.1
2500	10.768	10.285	9.232	8.75	3.688	13.593	22.505	26.193	73.9
3000	12.921	12.342	11.079	10.5	4.426	16.312	27.006	31.431	88.7
3500	15.075	14.399	12.925	12.25	5.163	19.03	31.507	36.669	103.5
4000	17.228	16.456	14.772	14	5.901	21.749	36.007	41.908	118.2

3.6.4 Effect of generator temperature on performance of ST cycle and VARS

Figs. 3.6(a) and 3.6(b) show the variation of power, SER and efficiency of the reheat regenerative ST cycle with generator temperature (T_G) of the VARS. It is observed from Fig. 3.6 (a) that the ST power and the net power do not vary much with T_G . Both ST power and net power show a marginal increase when T_G is increased from 70°C to 80°C which however decrease with further increase in T_G. At higher generator temperature, the steam from the ST is extracted at higher pressure and temperature. This is required for maintaining 10°C temperature difference for effective heat transfer to take place between the steam and the strong solution in the generator. Moreover the amount of extracted steam also increases slightly with increase in generator temperature (Fig. 3.6(a)) which would have otherwise produced some more power in the ST. The amount of steam required to be extracted at the desired pressure and temperature is found minimum at T_G =80°C, hence both the ST power and net power is the maximum at this temperature. The efficiency values also follow the same trend as that of the net power which is shown in Fig. 3.6 (b).

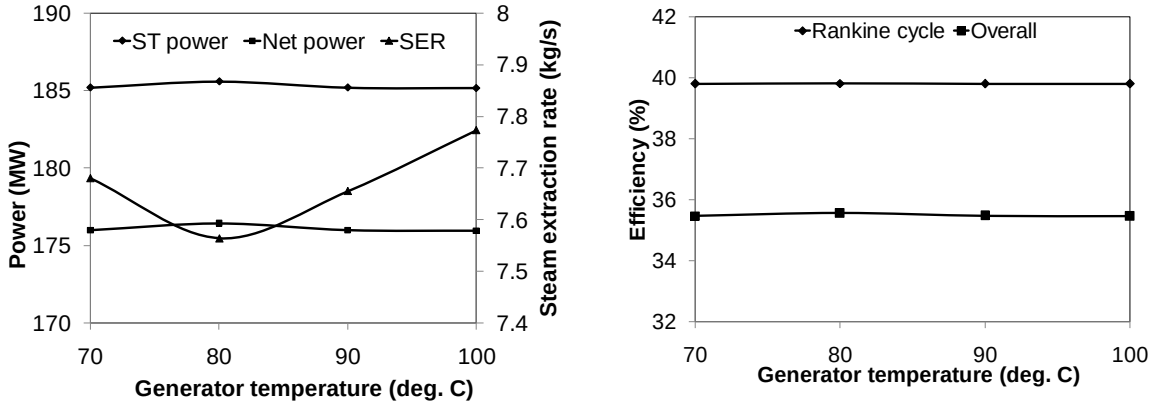

(a) (b)

Fig. 3.6: Effect of VARS generator temperature on (a) power, SER and (b) efficiency of the topping ST cycle

Table 3.6 shows the results corresponding to the performance of bottoming VARS as function of generator temperature. With absorber temperature (T_A), VARS condenser temperature (T_C) maintained at 35°C, evaporator temperature (T_E) at 10°C

and solution heat exchanger (SHE) efficiency of 75%, it is found that COP of the VARS increases from 0.799 at T_G =70°C to 0.813 at T_G =80°C and then it again starts decreasing with increase in T_G, hence is maximum at T_G =80°C. Variation of COP with T_G and T_G corresponding to maximum COP depends on selection of temperature values of the other components (T_C, T_E and T_A) and also the SHE efficiency as mentioned in Ref. [10]. Now, for the given T_C, T_E, T_A and SHE efficiency values in the present study, T_G corresponding to maximum COP is 80°C, however if we take say T_E =5°C T_A = T_C =35°C and SHE efficiency of 70%, as presented in Ref. [10], we get a different values of COP at various T_G, with maximum COP of 0.768 at 90°C. It is observed in Table 3.6 that the thermal loads in the generator and absorber ($\dot{Q}_A$) initially decreases when T_G increases from 70°C to 80°C, but at T_G =90°C and 100°C it again shows higher values. However, the thermal load in the VARS condenser ($\dot{Q}_C$) shows an increasing trend with T_G. As can be seen, the mass flow rate of refrigerant remains unchanged, but the mass flow rate of LiBr salt, weak and strong solution decreases with increase in T_G. Concentration of weak solution leaving the generator increases while that of the strong solution remains constant with T_G, therefore decrease in weak solution mass flow rate is obvious as per definition given in Equation (3.21). The mass flow rate of strong solution also decreases simultaneously and since the strong solution concentration remains constant, hence the required amount of LiBr salt reduces. With increasing T_G, the enthalpy of refrigerant vapours (state point $1'$), enthalpy of the weak solution (state point $8'$) leaving the generator and enthalpy of strong solution at entry to the generator (state point $7'$) increases, but since the mass flow rate of weak and strong solution decrease, so these changes finally lead to a variation of $\dot{Q}_G$ as given in Table 3.6 for the chosen values of T_C, T_E, T_A and SHE efficiency. Enthalpy at state points $4'$ and $5'$ is not changed although the enthalpy at state point $10'$ increases due to increase in T_G and concentration of weak solution. Accordingly with decreasing weak and strong solution mass flow rate, finally we find the same trend of $\dot{Q}_A$ variation with that of $\dot{Q}_G$. VARS condenser thermal load increases due to increase in enthalpy of refrigerant vapors at state point $1'$, however $\dot{Q}_E$ does not change with T_G. Of course this particular trend of variation of thermal loads in

various components of the VARS including the COP has a direct relationship with the operating values of T_C, T_E, T_A and SHE efficiency chosen for this variation.

Table 3.6: Variation of performance parameters of the H_2O–LiBr VARS with generator temperature

T_G (ºC)	COP	$\dot{Q}_G$ (MW)	$\dot{Q}_A$ (MW)	$\dot{Q}_C$ (MW)	$\dot{m}_{H_2O}$ (kg/s)	$\dot{m}_{LiBr}$ (kg/s)	$\dot{m}_{ws}$ (kg/s)	$\dot{m}_{ss}$ (kg/s)	SP power (Watt)
70	0.799	17.525	16.865	14.66	5.901	48.671	87.885	93.786	264.6
80	0.813	17.228	16.456	14.772	5.901	21.749	36.007	41.908	118.2
90	0.801	17.468	16.585	14.884	5.901	15.049	23.098	28.998	81.8
100	0.789	17.738	16.743	14.996	5.901	12.008	17.237	23.138	65.3

3.6.5 Effect of VARS condenser temperature on performance of ST cycle and VARS

Figs. 3.7(a) and 3.7(b) are representatives of variation of ST cycle power, SER and efficiency with VARS condenser temperature (T_C). That the power and efficiency of the combined power and cooling plant is not affected much by the variation in T_C can be seen from Figs 3.7(a) and 3.7(b). Slight reduction in power and efficiency is noticed when condenser temperature increases. Increase in T_C causes increase in the amount of steam to be extracted to the generator which in turn reduces the ST power slightly. Thermal load of the other system components of the VARS also increases with T_C; particularly the generator and the absorber (Refer Table 3.7). $\dot{Q}_E$ is however not affected due to change in T_C which remains constant as per the problem definition. Due to increase in $\dot{Q}_G$, slightly more amount of steam is required to be extracted for the generator at higher condenser temperature as shown in Fig. 3.7(a). Increase in thermal load of the VARS condenser and absorber causes increase in water flow rate to be circulated through these devices, hence the CT side pumping power requirement also increases slightly with increase in T_C. This causes slight reduction in the net power output and efficiency of the plant.

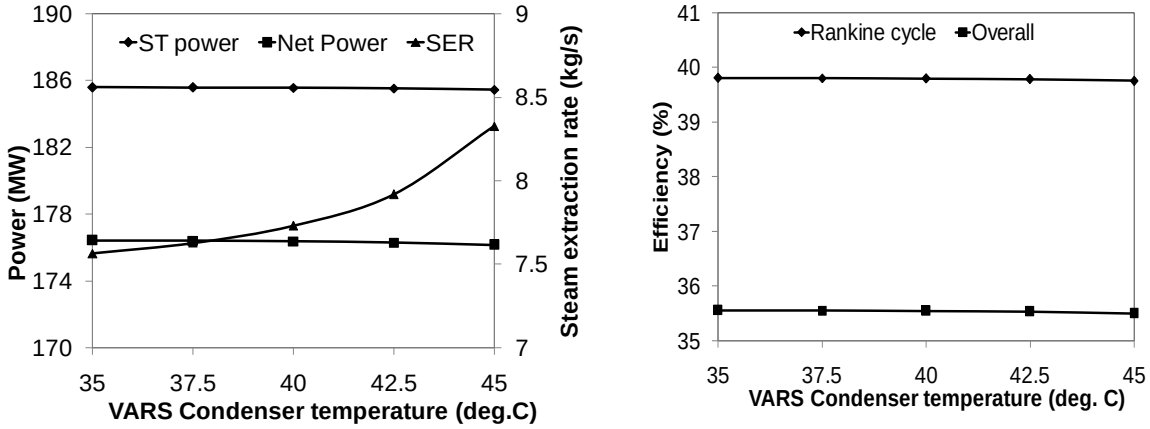

(a) (b)

Fig. 3.7: Effect of VARS condenser temperature on (a) power, SER and (b) efficiency of the topping ST cycle

Table 3.7 shows the performance results of the VARS due to variation in T_C. With increase in T_C, the VARS condenser operating pressure increases, thermal load in system components viz. $\dot{Q}_G$, $\dot{Q}_A$ and $\dot{Q}_C$ increases, increase in $\dot{Q}_C$ is very less compared to increase in $\dot{Q}_G$ and $\dot{Q}_A$. On the other hand, concentration of the weak solution decreases while that of the strong solution and evaporator thermal load '$\dot{Q}_E$' remains invariant with T_C. Enthalpy of refrigerant liquid at state point $2'$ (also at $3'$) increases, but the enthalpy of refrigerant vapour at state point $4'$ is not changed. Hence, the mass flow rate of refrigerant as defined in Equation (3.19) is more at higher T_C. Mass flow rate of weak and strong solution also increases due to increase mainly in the in refrigerant mass flow rate. SP power also increases with T_C due to increase in the condenser pressure and increase in mass flow rate of strong solution. $\dot{Q}_G$ and $\dot{Q}_A$ show an overall increase because of increase in mass flow rate of refrigerant, weak solution, strong solution and also due to increase in enthalpy of the working fluid at the relevant points of the bottoming VARS. Enthalpy at state point $2'$ increases whereas the same at state point $1'$ remains unchanged, so although the difference in enthalpy at state point $1'$ and $2'$ decreases but since mass flow rate of refrigerant increases, hence $\dot{Q}_C$ increases slightly with T_C. Since $\dot{Q}_G$ and SP power is more and also $\dot{Q}_E$ does not change, therefore COP of the VARS reduces at higher T_C.

Table 3.7: Variation of performance parameters of the H_2O–LiBr VARS with condenser temperature

T_C (ºC)	COP	$\dot{Q}_G$ (MW)	$\dot{Q}_A$ (MW)	$\dot{Q}_C$ (MW)	$\dot{m}_{H_2O}$ (kg/s)	$\dot{m}_{LiBr}$ (kg/s)	$\dot{m}_{ws}$ (kg/s)	$\dot{m}_{ss}$ (kg/s)	SP power (Watt)
35	0.813	17.228	16.456	14.772	5.901	21.749	36.007	41.908	118.2
37.5	0.806	17.371	16.597	14.774	5.927	25.707	43.609	49.536	166.0
40	0.795	17.606	16.829	14.777	5.953	31.711	55.152	61.105	241.2
42.5	0.776	18.032	17.253	14.779	5.979	41.906	74.771	80.751	372.7
45	0.738	18.963	18.181	14.782	6.006	63.054	115.494	121.501	651.7

3.6.6 Effect of evaporator temperature on performance of ST cycle and VARS

Evaporator temperature (T_E) also affects the performance of the topping ST cycle and bottoming VARS to a great extent. The effect of evaporator temperature on ST cycle power, efficiency and steam extraction rate is shown in Fig. 3.8(a) and Fig. 3.8(b). With increase in T_E, the ST power and net power both shows a marginal increase (Figs. 3.8 (a)). ST power increases marginally due to reduction in SER at higher evaporator temperature as shown in Fig. 3.8 (a). Therefore the amount of steam required for the VARS generator is less due to lower value of $\dot{Q}_G$ at higher T_E. Also lesser amount of cooling water is required to be circulated through the ST cycle condenser, absorber and condenser of the VARS due to which the pumping power requirement for the CT side pumps reduces to some extent; hence, there is a little gain in the net power and efficiency.

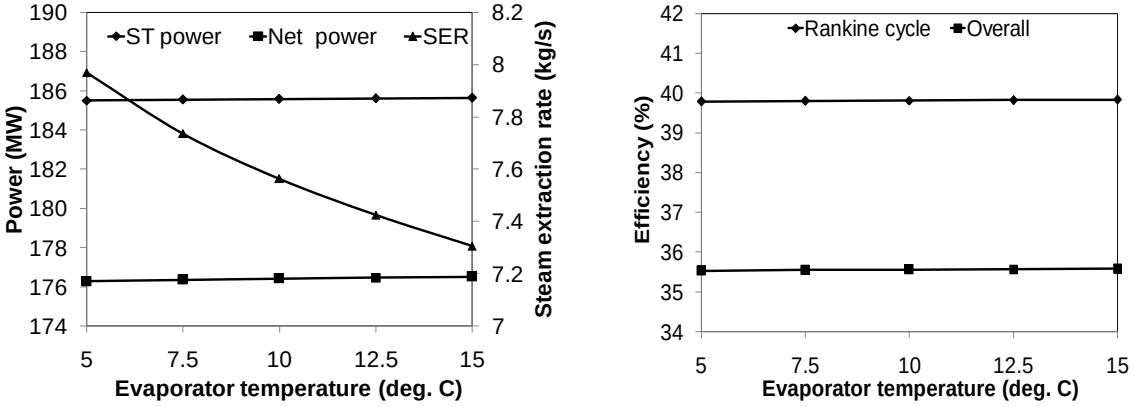

(a) (b)

Fig. 3.8: Effect of VARS evaporator temperature on (a) power, SER and (b) efficiency of the topping ST cycle.

As can also be seen from Table 3.8 is that the COP of the VARS is more at higher T_E. Effect of change in evaporator temperature 'T_E' on VARS performance is shown in Table 3.8. With increase in T_E, evaporator pressure increases, thermal load in the generator '$\dot{Q}_G$', condenser '$\dot{Q}_C$'and absorber '$\dot{Q}_A$', consumption rate of LiBr salt, mass flow rates of refrigerant, strong solution, and weak solution, SP power all reduces. Enthalpy of refrigerant vapour at state $4'$ increases while that of liquid refrigerant at states $1'$and $2'$ remain unaffected along with the evaporator CL $\dot{Q}_E$. Therefore the mass flow rate of refrigerant gets reduced due to which condenser thermal load '$\dot{Q}_C$' also decreases. Weak and strong solution flow rate decreases due to this and also due to decrease in concentration of the strong solution. Concentration of weak solution however remains constant with T_E variation. Enthalpy values at state points $5'$ and $7'$ reduces while at $8'$ and $10'$ it remains unchanged. Due to reduction in the mass flow rates of refrigerant, weak and strong solution and also enthalpy values at relevant state points, $\dot{Q}_G$ and $\dot{Q}_A$ values decrease with T_E as given in Table 3.8. Since $\dot{Q}_G$ and SP power is less and $\dot{Q}_E$ remains same, therefore finally the COP increases with increase in T_E.

Table 3.8: Variation of performance parameters of the H_2O–LiBr VARS with evaporator temperature

T_E (ºC)	COP	$\dot{Q}_G$ (MW)	$\dot{Q}_A$ (MW)	$\dot{Q}_C$ (MW)	$\dot{m}_{H_2O}$ (kg/s)	$\dot{m}_{LiBr}$ (kg/s)	$\dot{m}_{ws}$ (kg/s)	$\dot{m}_{ss}$ (kg/s)	SP power (Watt)
5	0.771	18.153	17.324	14.829	5.924	38.018	62.943	68.866	202.5
7.5	0.794	17.621	16.821	14.8	5.912	27.917	46.219	52.131	150.7
10	0.813	17.228	16.456	14.772	5.901	21.749	36.007	41.908	118.2
12.5	0.828	16.91	16.167	14.743	5.889	17.592	29.126	35.015	95.5
15	0.841	16.64	15.925	14.715	5.878	14.602	24.176	30.054	78.3

3.6.7 Effect of absorber temperature on performance of ST cycle and VARS

Variations of ST cycle power, SER and efficiency with absorber temperature are shown in Fig. 3.9 (a) and Fig. 3.9 (b). Similar variation is observed for the parameters as in case of VARS condenser temperature variation. Thermal load in the generator and absorber increases while it remains unchanged in the condenser and evaporator. As a result more steam is required to be extracted for the generator which reduces the ST power and the CT side pumping power is also more at higher T_A. Hence the net power and efficiency both reduces slightly with increase in T_A. The change in performance of the VARS due to T_A is presented in Table 3.9. With increase in T_A, concentration of the strong solution increases and also thermal load in generator and absorber viz. $\dot{Q}_G$ and $\dot{Q}_A$. Concentration of the weak solution, $\dot{Q}_C$, $\dot{Q}_E$ and mass flow rate of refrigerant are not affected due to change in T_A. However, consumption of LiBr salt, weak and strong solution mass flow rates become more at higher T_A. This is mainly due to increase in the concentration of the strong solution. Enthalpy of weak solution at state point $8'$ remains same while that of strong solution at $7'$ increases. This together with higher mass flow rates of strong and weak solution finally give higher $\dot{Q}_G$ value at increased T_A. Similarly increase in mass flow rates of strong solution, weak solution and enthalpy at states $5'$ and $10'$ is responsible for increase in $\dot{Q}_A$. SP power also increases with increase in T_A, therefore the COP becomes less at higher T_A. That COP reduces and thermal load in generator '$\dot{Q}_G$' and absorber '$\dot{Q}_A$' increases with T_A is also reported in ref. [10].

Table 3.9: Variation of performance parameters of the H_2O–LiBr VARS with absorber temperature

T_A (°C)	COP	$\dot{Q}_G$ (MW)	$\dot{Q}_A$ (MW)	$\dot{Q}_C$ (MW)	$\dot{m}_{H_2O}$ (kg/s)	$\dot{m}_{LiBr}$ (kg/s)	$\dot{m}_{ws}$ (kg/s)	$\dot{m}_{ss}$ (kg/s)	SP power (Watt)
35	0.813	17.228	16.456	14.772	5.901	21.749	36.007	41.908	118.2
37.5	0.803	17.433	16.661	14.772	5.901	26.937	44.597	50.497	140.3
40	0.791	17.695	16.923	14.772	5.901	34.648	57.364	63.265	173.2
42.5	0.775	18.071	17.299	14.772	5.901	47.318	78.34	84.241	227.2
45	0.748	18.722	17.95	14.772	5.901	71.991	119.188	125.089	332.3

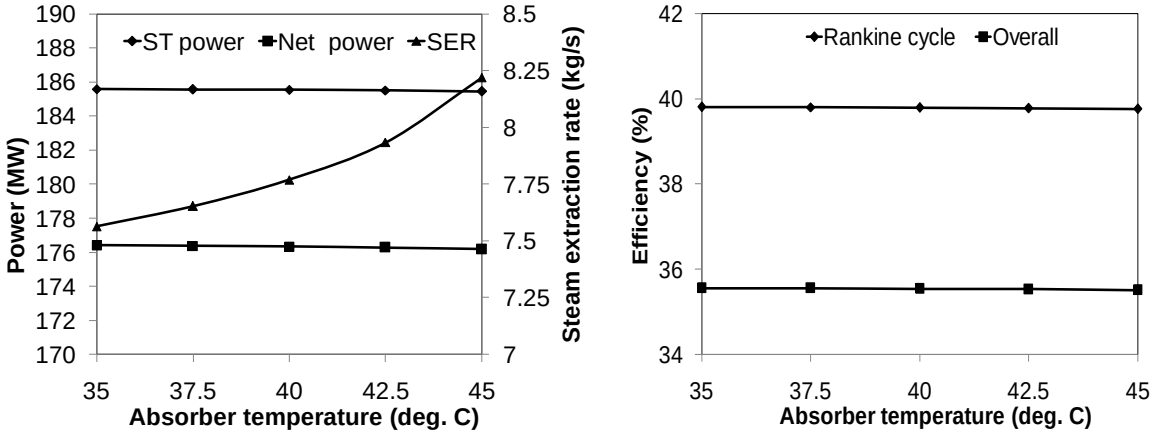

(a) (b)

Fig. 3.9 Effect of VARS absorber temperature on (a) power, SER and (b) efficiency of the topping ST cycle

3.6.8 Sensitivity analysis

A sensitive analysis is performed separately for comparative study on influence of the VARS operating temperatures, fuel flow rate and boiler pressure on VARS COP and net power of the topping ST plant. The comparison of sensitivity of COP and net plant power with respect to percentage change in the parameter values are shown in Table 3.10. Percentage changes are made with respect to operating conditions of T_G =80°C, T_C =35°C, T_E =10°C T_A =35°C, boiler pressure 150 bar, fuel flow rate 20 kg/s and

TOR=4000. From the results in Table 3.10 it is seen that the change in net power (also efficiency) with respect to change in VARS operating temperatures is very small. Influence of T_C and T_A are relatively more on COP compared to that of T_G and T_E. Fuel flow rate to boiler furnace and boiler pressure have no influence at all on COP of the VARS. As obviously the net power and efficiency of the topping cycle is more sensitive to the change in fuel flow rate, particularly the net power. Change in net power due to changes in boiler pressure with respect to the base case of 150 bar is not significant.

Table 3.10: Sensitivity of COP and net power with respect to change in VARS operating temperatures, fuel flow rate and boiler pressure (%)

Parameter	Changes in parameter (%)	Change in COP (%)	Change in net power (%)
T_G	10	–1.06	–0.02
	20	–2.31	–0.04
	30	–3.26	–0.05
T_C	10	–1.27	–0.02
	20	–3.88	–0.06
	30	–10.68	–0.19
T_A	10	–1.71	–0.03
	20	–4.18	–0.07
	30	–8.96	–0.15
T_E	10	0.79	0.01
	20	1.53	0.02
	30	2.23	0.03
Fuel flow rate	10	0.00	9.63
	20	0.00	19.13
	30	0.00	28.50
Boiler pressure	–33.33	0.00	–1.69
	–16.66	0.00	–0.32
	16.66	0.00	–0.01
	33.33	0.00	–0.35

3.6.9 Performance comparison of the combined power and VARS with the power cycle without VARS

In the previous sections (sub section 3.6.1 to sub section 3.6.7), the detailed performance analysis of the CPC system was provided. This section compares

the performance of the combined RRVPC and the single effect VARS with the ST cycle without VARS. Table 3.11 below shows the detailed results of comparison between the ST cycle with and without VARS. These results correspond to fuel flow rate of 20 kg s^{-1}, T_G =80°C, T_C =35°C, T_E =10°C, T_A =35°C and evaporator CL of 4000 TOR. It was seen that the net power output of the plant with VARS is less than the plant without VARS at all boiler pressures. This is mainly due to increase in the CT side pumping power with an additional pump installed between the mixing chamber and the CT. There is very little difference in BFP pumping power between the plant with and without VARS. BFP pumping power is slightly less in case of the plant with VARS due to steam extraction from the ST that is required for the VARS generator. As a result, the amount of water required to be pumped by the BFP reduces. Loss in ST power due to extraction of steam required for the VARS generator is more at higher boiler pressure but overall the impact is less because a little amount of steam is only extracted. The difference in the overall efficiency between the plant with and without VARS is also quite less.

3.6.10 Performance comparison of the ST cycle (without VARS) with CWH and without CWH

Water heaters are used in a regenerative plant to improve system efficiency. An attempt is made to investigate the effect of the CWH on performance of the ST plant (without VARS) while comparing it quantitatively with that of the plant without CWH. It can be seen from Table 3.12 that net power and efficiency of the plant with the CWH is more compared to the plant without CWH. This is because with the CWH incorporated, the enthalpy of water at inlet to the boiler increases and since the fuel flow rate supplied to the boiler furnace is same for both the cases with and without CWH, hence more amount of steam is produced that causes an increase in the net power and efficiency of the plant with the CWH. Although the BFP pumping power is more, but the CT side pumping power is less, however the overall total pumping power is more for the plant with CWH. But since the power produced by the ST is more due to higher steam generation capacity, hence there is an overall gain in the net power and efficiency. Gain in ST power and net power however decreases with increasing boiler pressure. Total pumping power of both the plants with and without CWH is more at higher boiler pressure. Compared to the plant without CWH, the increase in total pumping power with

boiler is more for the plant with CWH. This is the reason that the gain in net power and efficiency reduces with increasing boiler pressure.

3.7 Summary

The thermodynamic performance of a combined reheat regenerative vapour power cycle and LiBr based VARS has been simulated with the help of a numerical code written in C language. A detail parametric study is carried out to identify the importance of various operating parameters such as boiler pressure, fuel flow rate, evaporator CL and operating temperature of VARS components on performance of the combined power and cooling system. The parametric analysis based on variation of the above parameters yields a detailed insight about the influence of these variables on the overall system performance of the topping and bottoming cycle.

With fuel flow rate varied from 5 to 20 kg s^{-1} and boiler pressure from 100 to 200 bar, it is found that increase in both of these parameters results in increase of the steam generation capacity of the boiler. Net power and efficiency of the combined power and cooling plant is found to be the maximum at 150 bar. It is the net power which is more affected by variation in the boiler pressure and the fuel flow rate, the effect of variation of these parameters on efficiency is not very noticeable. The plant's net power shows a rapid increase during change of boiler pressure from 100 to 125 bar, but thereafter the gain in net power reduces and in fact the net power starts reducing at boiler pressure from 175 bar due to more pumping power requirement at higher boiler pressure. With fuel flow rate, the net power production of the plant varies from 43.813 MW at 5 kg s^{-1} to 176.418 MW at 20 kg s^{-1}. However, changes in boiler pressure and fuel flow rate have no effect on the performance of the bottoming VARS. On the other hand, changes in VARS evaporator CL and operating temperatures of the VARS components have their impact on both the power (topping) and cooling (bottoming) cycle.

Variation of VARS evaporator CL from 2000 to 4000 TOR indicates higher rate of steam extraction for the VARS generator, reduction in power and efficiency of the topping cycle at increased TOR. Increase in evaporator CL causes proportional increase in thermal load of all the VARS components, mass flow rate of refrigerant, lithium bromide salt, weak and strong solution and also the SP power. However the enthalpy at various state points and the COP of the VARS remain unchanged.

VARS generator temperature 'T_G' is another important parameter having its impact on both the power and the cooling cycle. Power and efficiency of the topping cycle changes with T_G and in the present study with the chosen operating temperatures of the other components and SHE efficiency, the maximum net power and efficiency is obtained at T_G =80°C. The COP of the VARS is also the maximum at T_G =80°C with minimum thermal load in the VARS generator and absorber. This is due to the amount of steam extracted from the ST as heat source for the VARS generator at 90°C which is the minimum at T_G =80°C. VARS condenser thermal load increases with T_G, while the evaporator CL, refrigerant mass flow rate, concentration of strong solution remains unchanged. Mass flow rates of LiBr salt, weak and strong solution decreases with increase in T_G due to decrease in concentration of weak solution at higher T_G. All these presented variations with respect to T_G may however be different at values of T_C, T_E, T_A and SHE efficiency other than what is chosen in the present study.

Table 3.11: Comparison of results between the combined RRVPC–VARS and the power cycle without VARS

Parameter	Boiler pressure (100 bar)		Boiler pressure (125 bar)		Boiler pressure (150 bar)		Boiler pressure (175 bar)		Boiler pressure (200 bar)	
	With VARS	Without VARS	With VARS	Without VARS	With VARS	Without VARS	With VARS	Without VARS	With VARS	Without VARS
Net power (MW)	173.433	180.785	175.852	186.477	176.418	188.759	176.393	189.329	175.795	189.331
BFP pumping power (kW)	2015.565	2021.804	2575.312	2583.137	3144.994	3154.428	3738.128	3749.238	4349.346	4362.179
CT side pumping power (kW)	6170.889	2814.908	6051.635	2726.666	6023.176	2678.916	6023.568	2679.596	6051.629	2696.596
Overall efficiency (%)	34.956	36.438	35.443	37.585	35.557	38.045	35.552	38.160	35.432	38.160
Loss of ST power due to VARS (MW)	4.003		4.725		5.852		5.855		5.831	

Table 3.12: Comparison of results between the ST based power cycle (without VARS) and the power cycle without CWH

Parameter	Boiler pressure (100 bar)		Boiler pressure (125 bar)		Boiler pressure (150 bar)		Boiler pressure (175 bar)		Boiler pressure (200 bar)	
	With CWH	Without CWH	With CWH	Without CWH	With CWH	Without CWH	With CWH	Without CWH	With CWH	Without CWH
Net power (MW)	180.785	172.355	186.477	175.868	188.759	177.876	189.329	178.087	189.331	177.682
BFP pumping power (kW)	2021.804	1661.955	2583.137	2124.968	3154.428	2590.195	3749.238	3074.098	4362.179	3566.086
CT side pumping power (kW)	2814.908	3063.896	2726.666	2958.41	2678.916	2899.214	2679.596	2893.039	2696.596	2904.896
Steam generation rate (kg/s)	166.844	133.867	168.662	135.679	170.498	137.272	172.459	138.929	174.566	140.494
Overall efficiency (%)	36.438	34.738	37.585	35.446	38.045	35.851	38.160	35.894	38.160	35.812
Gain of ST power due to CWH (MW)	8.541		8.252		8.072		7.955		7.874	

With increase in VARS condenser temperature, power and efficiency of the topping power cycle slightly reduces due to increase in the amount of steam to be extracted for the generator. In the bottoming cycle, concentration of the weak solution decreases while the strong solution concentration, evaporator CL remains unchanged with condenser temperature. Thermal load in VARS generator, condenser, absorber, mass flow rates of refrigerant, LiBr salt, weak solution and strong solution, SP power all increase with T_C, but the COP of the VARS reduces.

With evaporator temperature, net power and efficiency of the topping cycle shows a marginal increase and steam to be extracted for VARS generator reduces. VARS components' thermal load, mass flow rates of refrigerant, LiBr salt, weak and strong solution, SP power all reduces while the COP increases with increase in T_E.

The net power and efficiency of the power cycle reduces slightly with increase in absorber temperature T_A. Thermal load in the generator and absorber increases while it remains unchanged in the condenser and evaporator. Increase in concentration of the strong solution causes increase in consumption of LiBr salt, weak and strong solution mass flow rates at higher T_A. SP power also increases causing reduction in VARS COP.

Sensitivity analysis shows a very little change in net power and efficiency of the topping ST cycle with changes in VARS operating temperatures. Similarly fuel flow rate to boiler furnace and boiler pressure has no influence over the COP of the VARS. COP of the VARS is more sensitive to the change in T_C and T_A compared to change in T_G and T_E. Net power of the ST plant is highly sensitive to the change in fuel flow rate.

Comparison of performance of the power cycle with and without the VARS reveals that the net power output of the plant with VARS is comparatively less than the plant without VARS at all boiler pressures. This is mainly due to increase in CT side pumping power with one additional pump installed in the plant with VARS. There also exists very little difference in overall efficiency between the plant with and without VARS.

For the power plant without VARS, when the CWH is removed, it is found that the net power and efficiency reduces, however compared to efficiency, the loss in net

power output is more which however reduces with increase in boiler pressure. At a boiler pressure of 150 bar, the loss in power due to removal of CWH is as high as 5.339 MW.

Based on the results obtained it can be summarized that the steam extracted from a pass out steam turbine of a thermal power plant can be effectively used as a source of heat for the generator of a H_2O–LiBr VARS. This has more flexibility in terms of selection of the generator temperature which influences the performance of the both the power cycle and the VARS.

List of References

[1] Misra, R. D., Sahoo, P. K., Sahoo, S., and Gupta, A. Thermoeconomic optimization of a single effect water/LiBr vapour absorption refrigeration system. *International Journal of Refrigeration*, 6(2):158–169, 2003.

[2] Misra, R. D., Sahoo, P. K., and Gupta, A. Thermo–economic evaluation and optimization of a double–effect H_2O/LiBr vapour–absorption refrigeration system. *International Journal of Refrigeration*, 28(3):331–343, 2005.

[3] Misra, R. D., Sahoo, P. K., and Gupta, A. Thermoeconomic evaluation and optimization of an aqua–ammonia vapour–absorption refrigeration system. *International Journal of Refrigeration*, 29(1): 47–59,2006.

[4] Kaushik, S. C. and Singh, O. K. Estimation of chemical exergy of solid, liquid and gaseous fuels used in thermal power plants. *Journal of Thermal Analysis and Calorimetry*, 115:903–908, 2014.

[5] Nag, P. K. *Power Plant Engineering*. Tata McGraw Hill, New Delhi, India, 2nd edition, 2001.

[6] Kotas, T.J. The exergy method of thermal plant analysis. London: Butterworths; 1985.

[7] Lansing, F. L. Computer modelling of a single stage lithium bromide/water absorption refrigeration unit, JPL Deep Space Network progress Report 42–32, DSN Engineering section, 247–257, 1976.

[8] Wagner, W., Cooper, J.R., Dittmann, A., Kijima, J., Kretzschmar, H.J., and Kruse, A. The IAPWS Industrial Formulation 1997 for the thermodynamic properties of water and steam. *Journal of Engineering for Gas Turbines and Power*, 122:150–182, 2000.

[9] Patek, J.,and Klomfar, J. A computationally effective formulation of thermodynamic properties of LiBr–H_2O solutions from 273 to 500 K over full composition range. *International Journal of Refrigeration*, 29:566–578,2006.

[10] Kaynakli, O. and Kilic, M. Theoretical study on the effect of operating conditions on performance of absorption refrigeration system. *Energy Conversion and Management*, 48(2):599–607,2007.

[11] Dincer, I. and Al–Muslim, H. Thermodynamic analysis of reheat cycle steam power plants. *International Journal of Energy Research*, 25(8): 727–739, 2001.